Baker, H. S., Millar, R. J., Karoly, D. J., Beyerle, U., Guillod, B. P., Mitchell, D., Shiogama, H., Sparrow, S., Woollings, T., & Allen, M. R. (2018). Higher CO_2 concentrations increase extreme event risk in a 1.5 °c world. *Nature Climate Change*, *8*(7), 604-608. https://doi.org/10.1038/s41558-018-0190-1

Higher CO_2 concentrations increase extreme event risk in a 1.5°C world

Hugh S. Baker[1,*], Richard J. Millar[2], David J. Karoly[2,3,4], Urs Beyerle[5], Benoit P. Guillod[2,5,6], Dann Mitchell[7], Hideo Shiogama[8], Sarah Sparrow[9], Tim Woollings[1], and Myles R. Allen[1,2]

[1]Atmospheric, Oceanic and Planetary Physics, University of Oxford, Parks Road, Oxford, OX1 3PU, UK.

[2]Environmental Change Institute, School of Geography and the Environment, University of Oxford, South Parks Road, Oxford, OX1 3QY, UK.

[3]School of Earth Sciences, University of Melbourne, Melbourne, Australia.

[4]Australian Research Council Centre of Excellence for Climate System Science, Melbourne, Australia.

[5]Institute for Atmospheric and Climate Science, Swiss Federal Institute of Technology (ETH Zurich), Zurich, Switzerland.

[6]Institute for Environmental Decisions, Swiss Federal Institute of Technology (ETH Zurich), Zurich, Switzerland.

[7]School of Geographical Sciences, University of Bristol, University Rd, Bristol, BS8 1SS, UK.

[8]Center for Global Environmental Research, National Institute for Environmental Studies, 16-2 Onogawa, Tsukuba, Ibaraki 305-8506, Japan.

[9]Oxford e-Research Centre (OeRC), University of Oxford, Keble Road, Oxford, OX1 3QG, UK.

[*]hugh.baker@physics.ox.ac.uk

Summary

The Paris Agreement[1] aims to *'pursue efforts to limit the temperature increase to 1.5°C above pre-industrial levels.'* However, it has been suggested that temperature targets alone are unable to limit the risks associated with anthropogenic emissions[2,3]. Here, using an ensemble of model simulations, we show that atmospheric CO_2 increase - a more predictable consequence of emissions compared to global temperature increase - has a significant impact on Northern Hemisphere summer temperature, heat stress, and tropical precipitation extremes. Hence in an iterative climate mitigation regime aiming solely for a specific temperature goal, an unexpectedly low climate response may have corresponding 'dangerous' changes in extreme events. The direct impact of higher CO_2 concentrations on climate extremes therefore substantially reduces the upper bound of the carbon budget, and highlights the need to explicitly limit atmospheric CO_2 concentration when formulating allowable emissions. Thus, complementing global mean temperature goals with explicit limits on atmospheric CO_2 concentrations in future climate policy would reduce the adverse effects of high-impact weather extremes.

Main Body

The long-term goal of the Paris Agreement[1] aims to strengthen the global response to the threat of climate change by: *'Holding the increase in the global average temperature to well below 2°C above pre-industrial levels and to pursue efforts to limit the temperature increase to 1.5°C above pre-industrial levels, recognizing that this would significantly reduce the risks and impacts of climate change.'* To achieve the warming goal, the agreement implements an explicit temperature-based goal-driven regime, with which mitigation efforts are intended to be revised to over time. Therefore, no explicit long-term emissions targets are directly associated with the agreement aims, aside from the need to ultimately achieve a balance between net anthropogenic greenhouse gas sources and sinks into the atmosphere[4]. Since the Paris Agreement, there has been a call for research into impacts associated with 1.5°C and 2°C globally-average surface temperature anomalies[5,6]. However, previous work[2,3] suggests global mean temperature targets alone are unable to comprehensively limit the risks from anthropogenic emissions, and that global mean temperature is not the sole driver of changes in temperature and precipitation patterns[7–11] and extremes[12–14].

Here we isolate the direct effect of CO_2 concentration, investigating the difference between estimated likely (>66% probability that the value will lie within this range) upper and lower bounds on CO_2 concentrations leading to 1.5°C of global warming in 2100 for adaptive pathways to meet the Paris Agreement goals under climate response uncertainty[15]. We define the direct effect of CO_2 concentration as all the effects of CO_2 on climate beside those occurring through ocean warming but including feedbacks over land (e.g. from soil moisture), therefore excluding most of the global temperature change since the latter is to a large extent determined by ocean temperatures. We run five Atmospheric Model Intercomparison Project (AMIP) style ensembles[16] with HadAM3P and MIROC5: a present day ensemble

(2006-2015); three ensembles with sea surface temperature (SST) levels equivalent to 1.5°C global mean warming relative to 1850-1900 with low, best-estimate and high CO_2 concentrations; and a 2.0°C ensemble with best-estimate CO_2 concentrations and SSTs for a 2.0°C world. By considering the difference between high and low CO_2 concentration ensembles, we find substantial differences in the patterns of change in temperature and precipitation, pointing to an increase in extreme event likelihood. These differences could have important consequences if international climate policy does not seek to limit CO_2 concentrations and instead concentrate exclusively on the global mean temperature target. This idealised experimental design helps focus on the risks associated with different atmospheric CO_2 concentrations, consistent with different climate responses, after global temperatures have stabilised at approximately the same level. We also compare the results from HadAM3P and MIROC5 to results from CAM4 (see Methods for setups), drawing similar conclusions.

The differences in global mean temperature and precipitation between the five ensembles are presented in Table S1. Global mean temperature changes between the 1.5°C ensembles are small, as expected due to the prescribed SSTs, with only a 0.12°C difference between low and high CO_2 ensembles in HadAM3P and 0.11°C in MIROC5. Over land, these changes are slightly more pronounced. To correct for the differences in global mean temperature between low, best-estimate and high ensembles, we use a simple linear regression model (see Methods for details), fitting changes in variables to changes in global mean temperature and radiative forcing. Using the regression coefficients and global mean temperature difference between 1.5°C ensembles, we then adjust all variables to have a value associated with the global mean temperature in the best-estimate ensemble. This means all differences between the 1.5°C ensembles are due to the direct radiative forcing effect from differing CO_2 concentrations. All variables and figures (unless specified) for the rest of this study use the corrected ensembles (i.e. with the effect of the global mean temperature differences between the 1.5°C ensembles removed). The spatial patterns of change in

HadAM3P due to the direct radiative forcing effect are shown for several variables in Fig. S1 (and without temperature correction in Fig. S2). It may be argued that the SST pattern and CO_2 concentrations are physically inconsistent with each other, but the simulated atmosphere is still physically consistent within the model with its SSTs and CO_2 boundary conditions. The top of atmosphere radiative imbalances in our ensembles lie within the range of imbalances in the historical AMIP simulations (see Fig. S3), and so any conclusions we draw possess the same caveats as conclusions drawn from using the AMIP simulations.

We consider three extreme indices: $\overline{TX90p}$, the number of days per season exceeding the 90th percentile of daily maximum temperature in the present day ensemble; $\overline{WBGT95p}$, the number of degree months per year above the 95th percentile of wet-bulb globe temperature (WBGT) in the same month of the present day ensemble; and $\overline{R95p}$, the number of days per season where precipitation exceeds the 95th percentile of daily precipitation on wet days (>1mm/day) in the present day ensemble (see Methods for details). Differences between the high and low CO_2 concentration ensembles are shown for HadAM3P, MIROC5 and CAM4 in Figs. 1, S5 and S7 respectively (and without temperature corrections in Figs. S4, S6, S8). The stippling shows differences discernible against the decadal variability in the model (see Methods for details). We test for statistical significance at the 10% level using a two-sample Kolmogorov-Smirnov test; the hatching in Fig. S9 indicates significant changes in extreme indices in HadAM3P (maps for the other ensembles are not shown, but display similar hatching regions). Due to large ensemble sizes, we find significant changes across large regions of the globe. There is considerable spread in extreme indices in the CMIP5 models at the same temperatures[2]. We sub-sample the CMIP5 ensembles, computing the JJA TX90p when each model reaches 1.5°C under the RCP8.5 scenario. The differences in the spatial patterns of TX90p between models with low and high global mean temperature sensitivity to carbon emissions (see Fig. S10), support our findings that increases in CO_2 concentrations lead to increases in extreme temperature.

The WBGT, a heat stress metric and proxy for human discomfort[17,18], allows us to better quantify the impact of temperature extremes on humans. We consider changes in the extreme metric $\overline{WBGT95p}$ due to increases in CO_2. In JJA, increases are co-located with high population density areas in the Eastern US seaboard, central Europe, the Arabian Peninsula and North-East China and Korea. These regions are likely to experience increases in likelihood and severity of humid heatwaves under climate change[19]. Our results suggest these increases may be partly due to differences in atmospheric composition. Increases in population over the coming decades, combined with rising CO_2 concentrations, mean more people will be exposed to the extreme changes in WBGT[20] with potential economic impacts[21] and potentially drastic societal implications[22].

Area mean changes from present day are summarized in Fig. 2 (and without temperature correction in Fig. S11). Global mean changes in temperature and precipitation are shown, as well as land averaged Northern Hemisphere extratropical (NH_ET), 30°N-90°N, and tropical, 30°S-30°N, JJA changes for the mean and extreme indices. It is clear from the differences between high and low CO_2 ensembles that the area averaged changes in JJA means and extremes are highly significant in both the NH extratropics and tropics for $\overline{WBGT95p}$ and $\overline{TX90p}$. $\overline{R95p}$ changes are significant in HadAM3P (excluding the extreme NH extratropical precipitation), but not in MIROC5.

We compare the difference in extreme indices due to the range in CO_2 concentrations consistent with 1.5°C warming scenarios with the difference between the best-estimate CO_2 concentration cases at 2.0°C and 1.5°C global mean warming. The CO_2 induced differences as a percentage of the global mean warming induced differences for HadAM3P are shown for $\overline{TX90p}$ (Fig. 3a,b) and $\overline{WBGT95p}$ (Fig. 3c,d) (and without temperature correction in Fig. S12). In JJA, over the NH midlatitudes, there are regions where the differences due to CO_2 are greater than those due to the extra 0.5°C of global mean warming. For $\overline{R95p}$, we show the zonally averaged differences for ensemble means in the solid colours,

and individual ensembles member differences in the light colours (Fig. 3e,f) (and without temperature correction in Fig. S12). In both DJF and JJA, the differences due to CO_2 in the tropics are on the same order of magnitude as the differences due to the extra 0.5°C of global mean warming. The importance of CO_2 on driving tropical extreme precipitation is contrary to the extratropics where global mean warming is the main driver[23]. The comparisons for MIROC5 (Fig. S13, and without temperature correction in Fig. S14) vary from HadAM3P, with slightly lower magnitude, but nevertheless show substantial changes due to CO_2 concentration differences compared to differences due to the extra 0.5°C of global mean warming.

These results highlight that increases in extreme indices due to the direct effect of CO_2 have important implications on the upper limit of CO_2 that can be emitted in order to limit changes in specific costly climate extremes. If we accept a level of extreme index increase consistent with 1.5°C of global mean warming associated with the increased CO_2 in the best-estimate climate sensitivity case, we can ask what the upper bound of the carbon budget is that will keep extreme event likelihoods at this level. This will reduce the upper bound of the carbon budget, which is currently set by the uncertainty in the CO_2 emission levels which lead to 1.5°C of global mean warming. This allowable emissions uncertainty arises due to the global mean temperature response uncertainty[24].

Using the simple regression model (see Methods for details), we calculate how each extreme index varies with global mean temperature and CO_2 concentration. Taking the extreme index value at 1.5°C of global mean warming in the best-estimate climate sensitivity case, we can then compute pairs of values of global mean temperature and CO_2 concentration resulting in that same extreme index value. This allows us to determine an upper bound for the carbon budget consistent with this extreme index change, as illustrated by Fig. 4 (see caption for details). For $\overline{TX90p}$ (Fig. 4a), the decrease in the upper bound of the carbon budget is from 569 to 471 GtC, giving a 23^{+11}_{-12}% decrease in the uncertainty range of the carbon budget. For $\overline{WBGT95p}$ and $\overline{R95p}$ the new upper bounds are 450 GtC and 438 GtC, and reductions in uncertainty

are 28^{+6}_{-9}% and 31^{+13}_{-17}% respectively (Figs. 4b,c). Reductions due to regional $\overline{WBGT95p}$ changes are shown in Fig. S15. Besides Western Africa, all regions display a decreased upper bound. We stress that these reductions in the carbon budget are only estimates based on the results from the three models. The use of a larger number of climate models run under a similar experiment, if they were available, would allow us to quantify the reduction more accurately. With the full range of CMIP5 models, there would be a greater spread in the uncertainty of the new upper bound of the carbon budget. However, based on the magnitude of the reduction in the upper bound of the carbon budget from these three models, it seems likely that the direct CO_2 effect is important, and should be taken into consideration when formulating carbon budgets to avoid any given level of climate impacts on extremes.

We demonstrate significant differences in temperature and precipitation extremes between the higher and lower likely CO_2 concentrations in a 1.5°C world. This highlights the importance of direct, local, CO_2 forcing effects on regional climates and extremes. We must acknowledge these effects so that we can avoid 'dangerous' changes in extremes which, in the context of the Paris Agreement, are defined as impacts beyond those expected at 1.5°C. It also makes clear that impacts on extremes in a world warming past 1.5°C would be different from those after stabilising at 1.5°C.

Differences in extremes at the same global mean temperature, due purely to differing CO_2 concentrations, directly impact the use of the pattern scaling technique[25]. These differences provide compelling evidence that when using pattern scaling, we must account for CO_2 concentration and not just the changes in global mean temperature (which is the dominant method used in academic and policy work).

This study supports findings[26] that geoengineering schemes aimed at reducing the global warming impacts without reducing CO_2 concentration would not fully mitigate changes in extremes whose likelihoods have increased by the direct effect of increasing CO_2 concentrations.

Whilst it is important to note these findings are from only three models, the use of large ensembles

and the statistical significance of the differences give weight to the reliability of our findings. Previous work[11] shows the rapid regional precipitation response to increases in CO_2 is robust among CMIP5 models. Further work must be carried out to explore the spatial patterns and magnitudes of temperature and precipitation differences in other models to better quantify how extremes change with different atmospheric CO_2 concentrations. Despite this, it is clear that complementing global mean temperature goals with explicit limits on atmospheric CO_2 concentrations would reduce the risk of unexpectedly high changes in high-impact weather extremes.

Acknowledgements

H.S.B. is supported by the Natural Environment Research Council grant NE/L002612/1. R.J.M. was supported by Natural Environment Research Council grant NE/P014844/1. D.M. is supported by a NERC independent fellowship. H.S. was supported by the Integrated Research Program for Advancing Climate Models (TOUGOU program) from the Ministry of Education, Culture, Sports, Science and Technology, Japan and ERTDF 2-1702 of Environmental Restoration and Conservation Agency, Japan. The authors thank the HAPPI project team and the modelling centers who contributed simulations. This research used science gateway resources of the National Energy Research Scientific Computing Center, a DOE Office of Science User Facility supported by the Office of Science of the U.S. Department of Energy under Contract No. DE-AC02-05CH11231. The authors are grateful to Friederike Otto for making available results from event attribution experiments that provided the original motivation for this study. We would like to thank our colleagues at the Oxford eResearch Centre: A. Bowery, M. Rashid, S. Sparrow, P. Uhe and D. Wallom for their technical expertise. We would like to thank the Met Office Hadley Centre PRECIS team for their technical and scientific support for the development and application of weather@Home. Finally, we would like to thank all of the volunteers who have donated their computing time to climateprediction.net and

weather@home.

Author contributions statement

M.R.A. conceived the experiment. S.S ran the HadAM3P simulations, H.S. ran the MIROC5 simulations, and U.B. ran the CAM4 simulations. H.S.B. performed the analysis with input from D.J.K., R.J.M., B.P.G., T.W., D.M. and M.R.A.. R.J.M. contributed to one of the figures. H.S.B. wrote the paper with comments from all the authors.

Additional information

Reprints and permissions information is available at www.nature.com/reprints. The authors declare no competing interests. Correspondence and requests for materials should be addressed to H.S.B. (hugh.baker@physics.ox.ac.uk).

References

1. United Nations/Framework Convention on Climate Change. *Adoption of the Paris Agreement* (21st Conference of the Parties, Paris: United Nations., 2015).

2. Seneviratne, S. I., Donat, M. G., Pitman, A. J., Knutti, R. & Wilby, R. L. Allowable CO2 emissions based on regional and impact-related climate targets. *Nat.* **529**, 477–483 (2016). URL http://www.nature.com/doifinder/10.1038/nature16542. DOI 10.1038/nature16542.

3. Steinacher, M., Joos, F. & Stocker, T. F. Allowable carbon emissions lowered by multiple climate targets. *Nat.* **499**, 197–201 (2013). URL https://www.nature.com/nature/journal/v499/n7457/pdf/nature12269.pdf. DOI 10.1038/nature12269.

4. Fuglestvedt, J. *et al.* Implications of possible interpretations of 'greenhouse gas balance' in the Paris Agreement. *Philos. Trans. A. Math. Phys. Eng. Sci.* **376**, 20160445 (2018). URL http://www.ncbi.nlm.nih.gov/pubmed/29610378. DOI 10.1098/rsta.2016.0445.

5. Mitchell, D. *et al.* Realizing the impacts of a 1.5C warmer world. *Nat. Clim. Chang.* **6**, 735–737 (2016). URL http://www.nature.com/doifinder/10.1038/nclimate3055. DOI 10.1038/nclimate3055.

6. Schleussner, C.-F. *et al.* Science and policy characteristics of the Paris Agreement temperature goal. *Nat. Clim. Chang.* **6**, 827–835 (2016). URL https://www.nature.com/nclimate/journal/v6/n9/full/nclimate3096.html. DOI 10.1038/nclimate3096.

7. Folland, C. K. *et al.* Influences of anthropogenic and oceanic forcing on recent climate change. *Geophys. Res. Lett.* **25**, 353–356 (1998). URL http://doi.wiley.com/10.1029/97GL03701. DOI 10.1029/97GL03701.

8. Sexton, D. M. H., Grubb, H., Shine, K. P. & Folland, C. K. Design and Analysis of Climate Model Experiments for the Efficient Estimation of Anthropogenic Signals. *J. Clim.* **16**, 1320–1336 (2003). URL http://journals.ametsoc.org/doi/abs/10.1175/1520-0442-16.9.1320. DOI 10.1175/1520-0442-16.9.1320.

9. Bony, S. *et al.* Robust direct effect of carbon dioxide on tropical circulation and regional precipitation. *Nat. Geosci.* **6**, 447–451 (2013). URL http://www.nature.com/doifinder/10.1038/ngeo1799. DOI 10.1038/ngeo1799.

10. Dong, B. & Sutton, R. Dominant role of greenhouse-gas forcing in the recovery of Sahel rainfall. *Nat. Clim. Chang.* **5**, 757–760 (2015). URL http://www.nature.com/doifinder/10.1038/nclimate2664. DOI 10.1038/nclimate2664.

232 **11.** Richardson, T. B., Forster, P. M., Andrews, T. & Parker, D. J. Understanding the Rapid Precipitation
233 Response to CO2 and Aerosol Forcing on a Regional Scale*. *J. Clim.* **29**, 583–594 (2016). URL http:
234 //journals.ametsoc.org/doi/10.1175/JCLI-D-15-0174.1. DOI 10.1175/JCLI-D-
235 15-0174.1.

236 **12.** Kamae, Y., Shiogama, H., Watanabe, M. & Kimoto, M. Attributing the increase in Northern
237 Hemisphere hot summers since the late 20th century. *Geophys. Res. Lett.* **41**, 5192–5199 (2014).
238 URL http://doi.wiley.com/10.1002/2014GL061062. DOI 10.1002/2014GL061062.

239 **13.** Seneviratne, S. I., Donat, M. G., Mueller, B. & Alexander, L. V. No pause in the increase of hot
240 temperature extremes. *Nat. Clim. Chang.* **4**, 161–163 (2014). URL http://www.nature.com/
241 doifinder/10.1038/nclimate2145. DOI 10.1038/nclimate2145.

242 **14.** Dong, B. *et al.* Abrupt summer warming and changes in temperature extremes over Northeast Asia
243 since the mid-1990s: Drivers and physical processes. *Adv. Atmos. Sci.* **33**, 1005–1023 (2016). URL
244 http://link.springer.com/10.1007/s00376-016-5247-3. DOI 10.1007/s00376-
245 016-5247-3.

246 **15.** Millar, R. J. *et al.* Emission budgets and pathways consistent with limiting warming to 1.5C. *Nat.*
247 *Geosci.* (2017). URL http://www.nature.com/doifinder/10.1038/ngeo3031. DOI
248 10.1038/ngeo3031.

249 **16.** Taylor, K. E., Stouffer, R. J. & Meehl, G. A. An Overview of CMIP5 and the Experiment Design.
250 *Bull. Am. Meteorol. Soc.* **93**, 485–498 (2012). URL http://journals.ametsoc.org/doi/
251 abs/10.1175/BAMS-D-11-00094.1. DOI 10.1175/BAMS-D-11-00094.1.

252 **17.** Sherwood, S. C. & Huber, M. An adaptability limit to climate change due to heat stress. *Proc. Natl.*
253 *Acad. Sci. U. S. A.* **107**, 9552–5 (2010). URL http://www.ncbi.nlm.nih.gov/pubmed/

20439769. DOI 10.1073/pnas.0913352107.

18. Willett, K. M. & Sherwood, S. Exceedance of heat index thresholds for 15 regions under a warming climate using the wet-bulb globe temperature. *Int. J. Clim.* **32**, 161–177 (2012). URL http://doi.wiley.com/10.1002/joc.2257. DOI 10.1002/joc.2257.

19. Russo, S., Sillmann, J. & Sterl, A. Humid heat waves at different warming levels. *Sci. Rep.* **7**, 7477 (2017). URL http://www.nature.com/articles/s41598-017-07536-7. DOI 10.1038/s41598-017-07536-7.

20. Im, E.-S., Pal, J. S. & Eltahir, E. A. B. Deadly heat waves projected in the densely populated agricultural regions of South Asia. *Sci. Adv.* **3** (2017). URL http://advances.sciencemag.org/content/3/8/e1603322.

21. Takakura, J. *et al.* Cost of preventing workplace heat-related illness through worker breaks and the benefit of climate-change mitigation. *Environ. Res. Lett.* **12**, 064010 (2017). URL http://stacks.iop.org/1748-9326/12/i=6/a=064010?key=crossref.0d43d24cc18b91bfe0bc7352a3d62165. DOI 10.1088/1748-9326/aa72cc.

22. Murari, K. K. *et al.* Intensification of future severe heat waves in India and their effect on heat stress and mortality. *Reg. Environ. Chang.* **15**, 569–579 (2015). URL http://link.springer.com/10.1007/s10113-014-0660-6. DOI 10.1007/s10113-014-0660-6.

23. Pendergrass, A. G., Lehner, F., Sanderson, B. M. & Xu, Y. Does extreme precipitation intensity depend on the emissions scenario? *Geophys. Res. Lett.* **42**, 8767–8774 (2015). URL http://doi.wiley.com/10.1002/2015GL065854. DOI 10.1002/2015GL065854.

24. IPCC. *Climate change 2013: The physical science basis* (Cambridge University Press, 2013b, 2014). URL http://www.epa-pictaural.com/ctr/m/cc/transcript/stocker.pdf.

276 **25.** Tebaldi, C. & Arblaster, J. M. Pattern scaling: Its strengths and limitations, and an update on the
277 latest model simulations. *Clim. Chang.* **122**, 459–471 (2014). URL http://link.springer.
278 com/10.1007/s10584-013-1032-9. DOI 10.1007/s10584-013-1032-9.

279 **26.** Curry, C. L. *et al.* A multimodel examination of climate extremes in an idealized geoengineering
280 experiment. *J. Geophys. Res. Atmos.* **119**, 3900–3923 (2014). URL http://doi.wiley.com/
281 10.1002/2013JD020648. DOI 10.1002/2013JD020648.

Figure captions

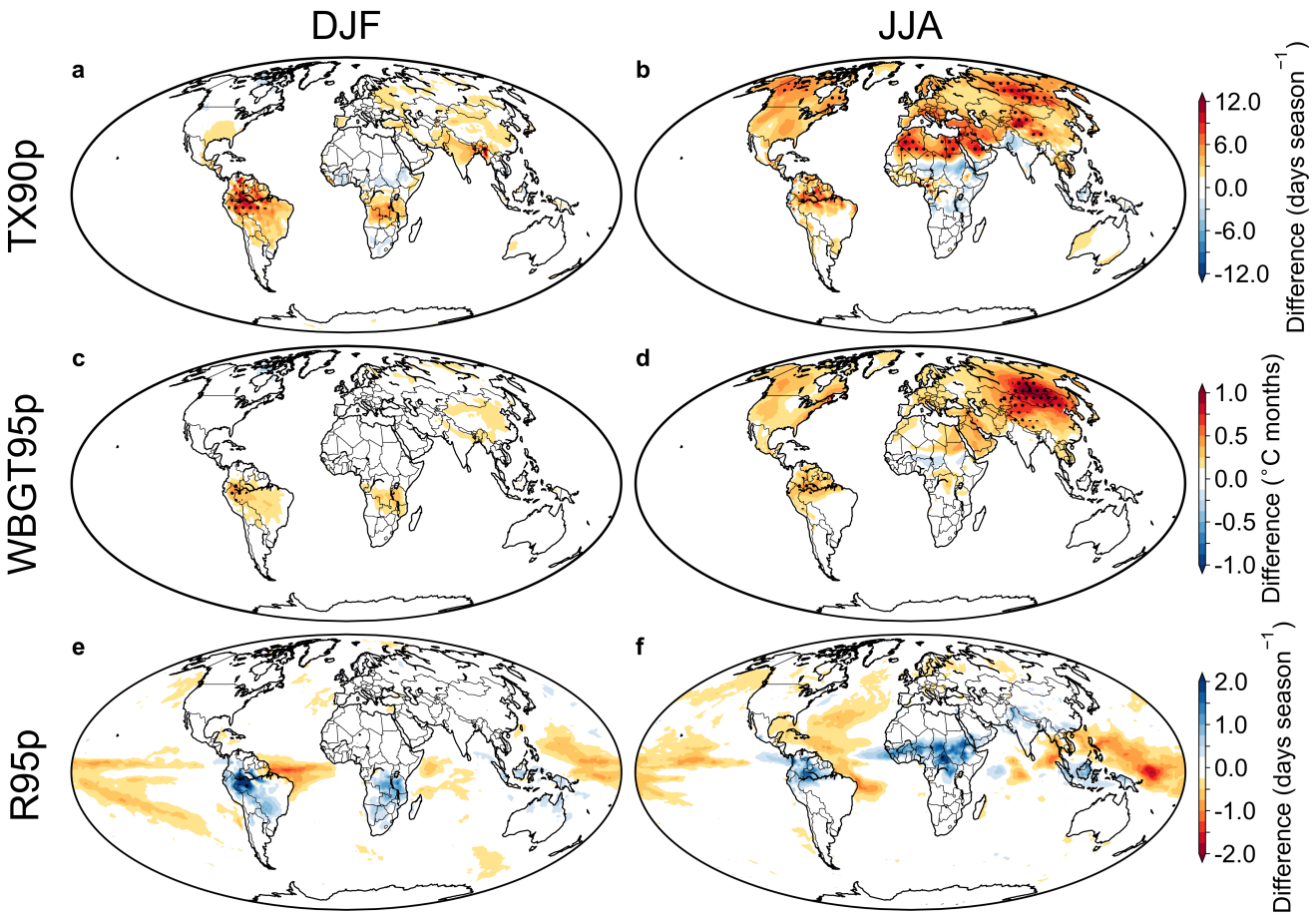

Figure 1. Changes associated with CO_2 concentration at 1.5°C warming in HadAM3P with temperature correction applied. Differences in $\overline{TX90p}$ (a, b), $\overline{WBGT95p}$ (c, d) and $\overline{R95p}$ (e, f) between high and low CO_2 forced runs. Stippling indicates statistical significance at the 10% level when testing for discernible impact (i.e. with an effective sample size of one, see Methods for details). Note the reversal of the colourbar for e, f.

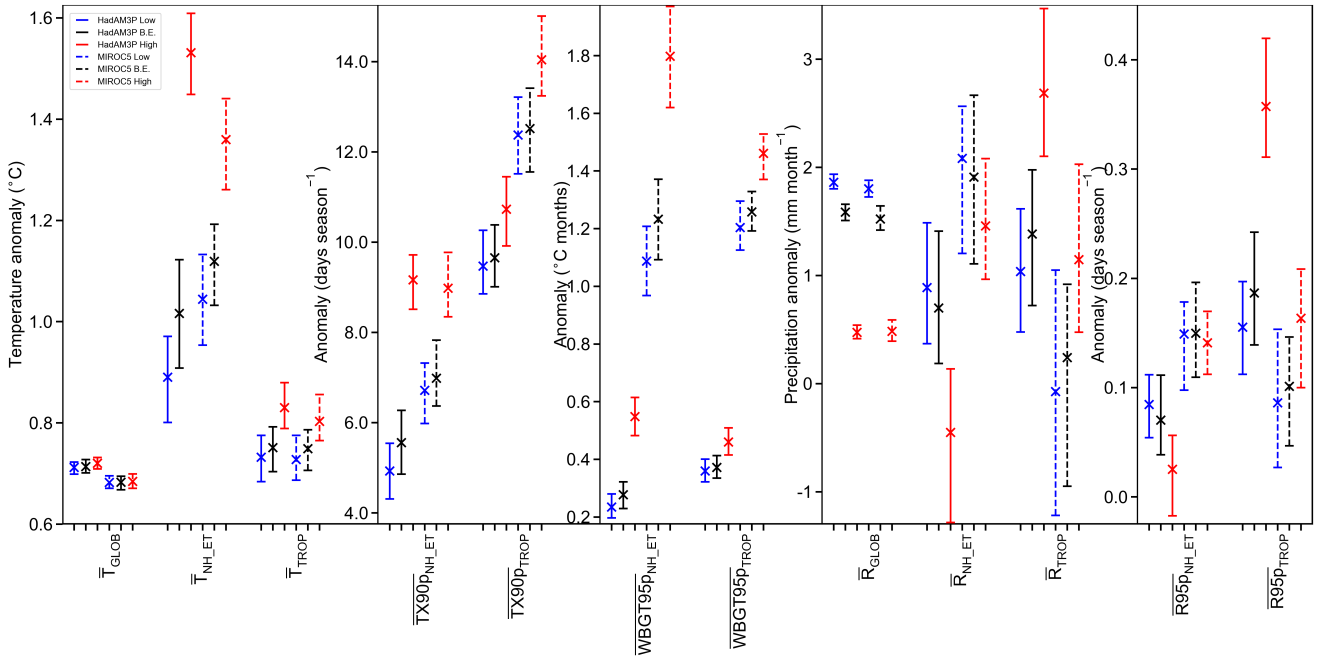

Figure 2. Area averaged differences associated with CO_2 concentration at 1.5°C warming with temperature correction applied. Whisker plots show the difference in indices between the low, best estimate and high CO_2 ensembles relative to the present day ensemble (solid lines: HadAM3P, dashed lines: MIROC5). Crosses mark the 50th percentile and the caps mark the 10th and 90th percentiles. Global mean temperature differences are calculated averaged over all seasons and the whole globe. 'NH_ET' indices are calculated for JJA 30°-90°N land,'TROP' indices are calculated for JJA 30°S-30°N land. Precipitation anomalies are expressed as the mean change at each gridpoint.

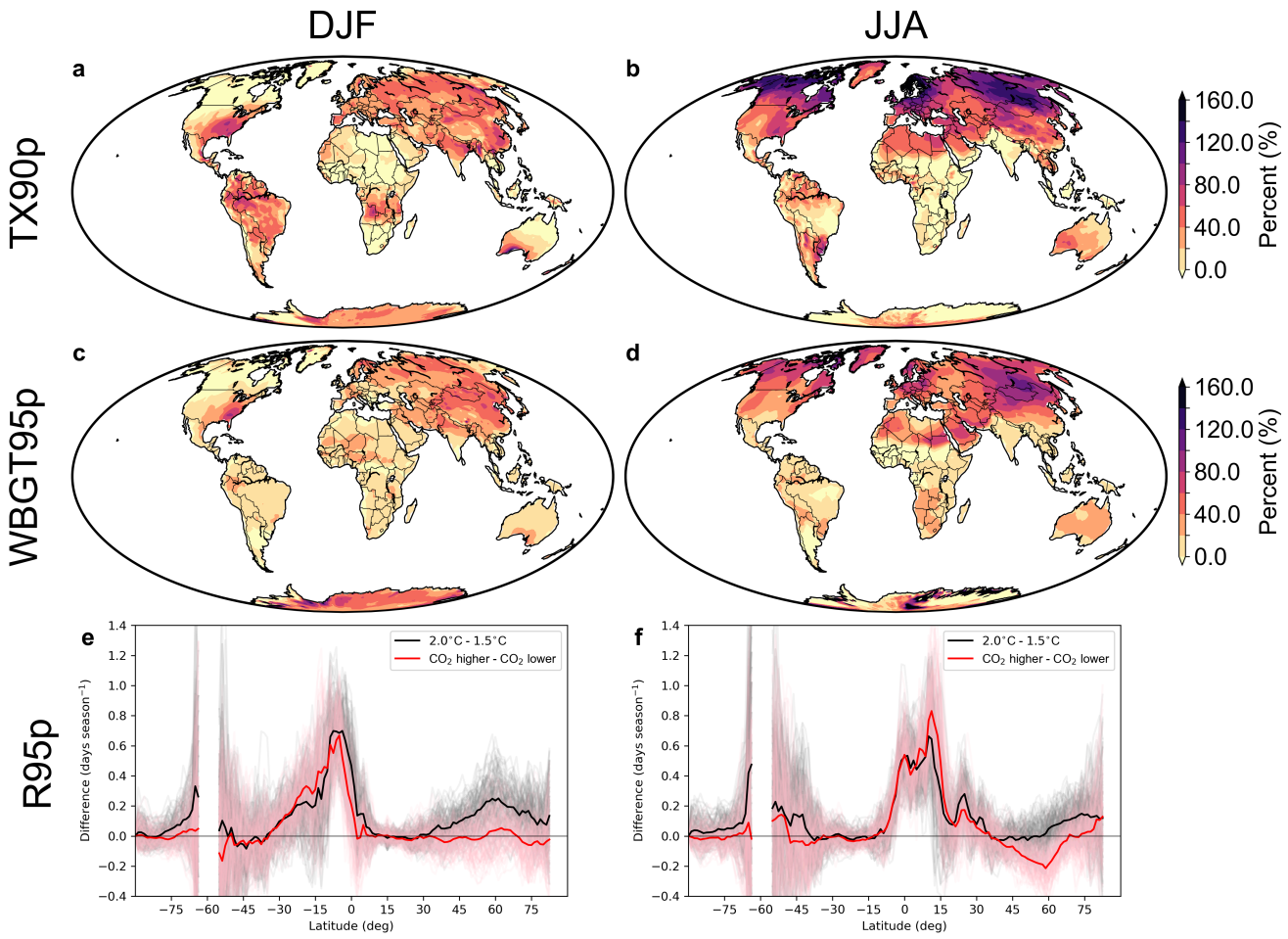

Figure 3. Comparison of changes due to CO_2 concentration with changes due to 2.0°C to 1.5°C warming difference in HadAM3P. Differences between high and low CO_2, with temperature correction applied, as a percentage of the difference between 2.0°C and 1.5°C ensembles for $\overline{TX90p}$ (a, b) and $\overline{WBGT95p}$ (c, d). The differences between high and low CO_2, and the differences between 2.0°C and 1.5°C for $\overline{R95p}$ (e, f). Plots show the zonally averaged mean ensemble $\overline{R95p}$ changes in solid colours, and individual ensemble members in the light colours.

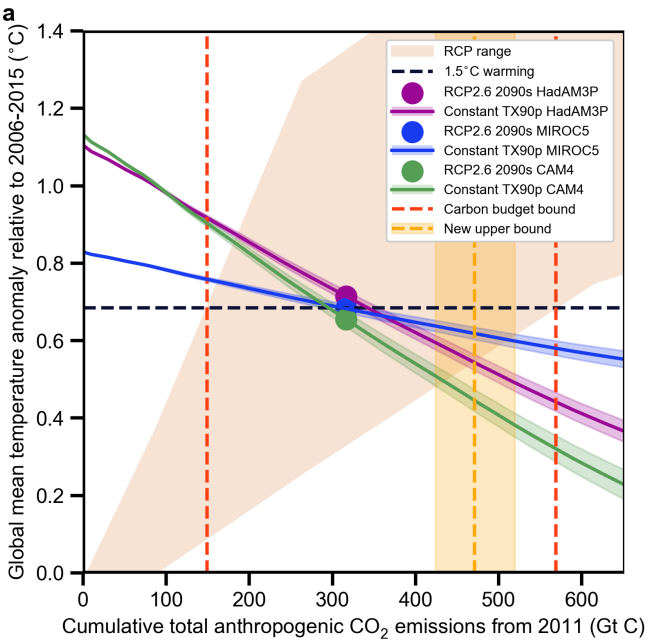

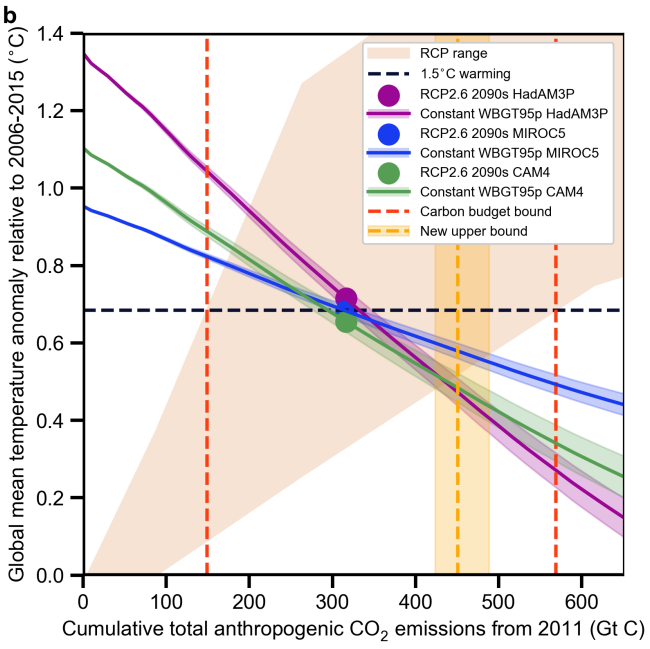

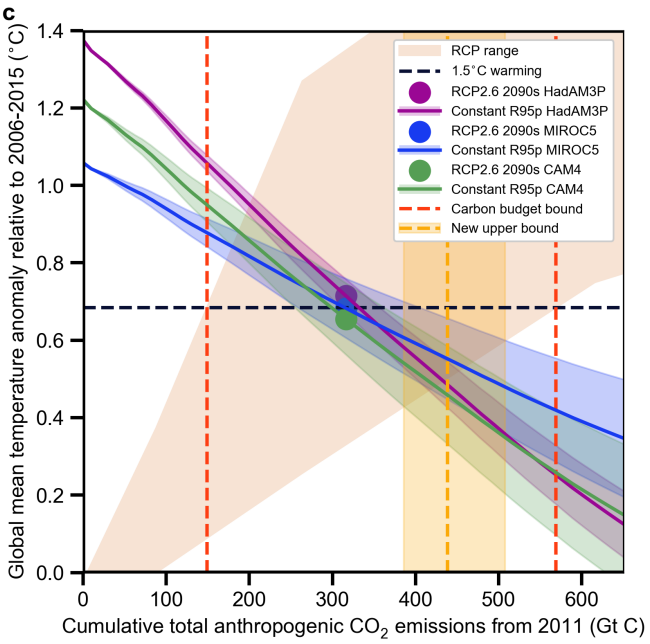

Figure 4. The reduction in the upper bound of the carbon budget. $\overline{TX90p}$ (JJA 30°-90°N land) (a), $\overline{WBGT95p}$ (JJA 30°-90°N land) (b) and $\overline{R95p}$ (JJA 30°S-30°N land) (c). The pink plume shows the 5-95 percentile of the CMIP5 response under all four RCPs relative to the 2006-2015 mean. The black dashed line marks the warming from the present decade equivalent to 1.5°C of mean global warming from the pre-industrial period (1850-1900). Dots indicate the warming observed in our best-estimate CO_2 concentration ensemble for each model (corresponding to the RCP2.6 2090-2099 mean). Curves show lines of constant extreme index, calculated from the regression model, with 5-95% uncertainty plumes. Red dashed lines mark the upper and lower uncertainty bounds of the carbon budget. The yellow dashed line is the new multi-model mean upper bound in the carbon budget, with uncertainty plume given by the pink plume's intersection with the model 5th percentile that gives the largest reduction in the carbon budget, to the intersection with the model 95th percentile that gives the smallest reduction in the carbon budget.

Methods

Experimental design

For this study, we make use of three climate models: HadAM3P, MIROC5[27] and CAM4[28]. HadAM3P is an atmosphere only, medium resolution, GCM developed by the UK Met Office. It is based upon the atmospheric component of HadCM3[29,30]. An improved version of HadAM3P using a more sophisticated land-surface scheme is used here[31]. The model has been used extensively in the study of extreme events. We run HadAM3P using the large-ensemble capability provided by the climate*prediction*.net volunteer computing network[31,32], where members of the public are performing multi-thousand-member initial condition ensemble general circulation model (GCM) simulations at 1.25° x 1.875° resolution. We compare the results from HadAM3P to MIROC5 and CAM4 run at 1.4° x 1.4° and 1.9° x 2.5° resolutions respectively.

The experimental setup follows the Half a degree Additional warming, Prognosis and Projected Impacts (HAPPI; www.happimip.org) design[33]. Forcing conditions are as in the DECK AMIP design, including SSTs and sea ice[16]. The HAPPI experiments are designed to simulate conditions in the present decade (2006-2015), and 1.5°C and 2.0°C warmer than pre-industrial (1861-1880) conditions. SSTs for the 1.5°C case are calculated by adding to the observed 2006–2015 SSTs a change in SST (ΔSST) between the decadal average of the modelled 2006–2015 period and the decadal average of the modelled 1.5°C world over 2091–2100[33]. Hence the SST patterns are still time varying because they are based on the 2006–2015 observations, but they have an additional warming added to them. As CMIP5 historical simulations stopped in 2005, the decadal average of the 2005–2015 SSTs is estimated from RCP8.5 simulations, as this is the scenario that is closest to observations over this period. The decadal average of the 2091–2100 SSTs is estimated from CMIP5 RCP2.6 simulations. The process to calculate the 2.0°C

SST pattern is similar and outlined in detail in reference [33]. Here we use the HAPPI Tier 1 experimental design[33], which uses the multi-model mean patterns, thus across all three models used in this study all the present day ensembles are run with an identical present day SST pattern, all the 1.5°C ensembles are run with an identical 1.5°C SST pattern, and all the 2.0°C ensembles are run with an identical 2.0°C SST pattern. Full details are discussed in reference [33].

For HadAM3P, we run five ensemble experiments, each over a 10-year period. A present day ensemble is run using HAPPI present day setup[33] over the period 2006-2015 with an average CO_2 of 390.4ppm (90 ensemble members). A 1.5°C ensemble is run using HAPPI 1.5°C setup[33], which uses the RCP2.6 forcing scenario boundary conditions from the last decade of the 21st century, with CO_2 fixed at 423.1ppm (71 members). Two further ensembles are run using the 1.5°C setup[33], but with CO_2 fixed at 395.8ppm and 550.0ppm (76 and 88 members) to represent the lower and higher likely CO_2 concentrations averaged over 2091-2100 in adaptive pathways that succeed in achieving warming below 1.5°C in 2100 for the assessed ranges of climate response uncertainty[15]. The range of CO_2 concentration is intended to illustrate the scale of the difference in concentrations that may be consistent with a 1.5°C world. Thus the range of concentrations used does not affect the qualitative results of changes in extremes. As the concentrations are only used to fit the regression model and not calculate changes in the carbon budget directly, the reduction in the upper bound of the carbon budget is not influenced by the exact choice of CO_2 concentrations. It is however influenced by the selection of models used in the study, due to their different climate sensitivities. A similar range in concentrations can be obtained by converting the spread of individual model temperatures in CMIP5 under RCP2.6 at the end of the century (2081-2100) to a concentration range. The change in temperature at the end of the century from the pre-industrial baseline stated in AR5[24] is 1.6°C with a standard deviation of 0.4°C and 5-95% uncertainty range of 0.9-2.3°C. The radiative forcing averaged over 2081-2100 is 2.60 Wm^{-2}, from which we compute the ratio of temperature to

radiative forcing. When multiplied by 1.5°C and converted to a concentration range, this gives a range of 400.2-510.2 ppm using the range of temperatures associated with one standard deviation from the mean, or 381.6-624.7 ppm when using the 5-95% range. A 2.0°C ensemble is run with the HAPPI 2.0°C SST pattern[33] and CO_2 fixed at 486.6ppm (96 members). All CO_2 concentrations are prescribed as a global mean atmospheric concentration. Following previous work[34], initial condition perturbations are applied between ensemble members via perturbations to the potential temperature. For MIROC5, we perform exactly the same ensemble runs, with 50 members per experiment using the same CO_2 concentrations as HadAM3P. For CAM4, we use the data from three experiments, a present day, 1.5°C, and 1.5°C with a CO_2 concentration of 379.0ppm (thus for CAM4, the 1.5°C ensemble with CO_2 at 423.1ppm doubles as the 'best-estimate' and 'high' ensembles and the 1.5°C with CO_2 at 379.0ppm becomes the 'low' ensemble), all using the HAPPI experimental design with 501 ensemble members.

Following standard AMIP design protocol[16], soil moisture is allowed to vary freely in our simulations. The primary aim of the study is to disentangle the direct CO_2 effect on regional climate from the ocean warming, since the latter strongly affects global mean warming and, additionally, may cause some large scale circulation changes. SST patterns can contribute to regional climate variability far further afield than their perturbation, whereas soil moisture effects are more local and do not affect global mean temperature significantly[35]. Some of the regional effect (and indeed perhaps a large part of this effect over land areas[35]) is due to changes in soil moisture. Holding soil moisture constant would mask some of the changes due to the direct effect of CO_2, preventing us from disentangling this effect from that of the global mean warming of the ocean.

We select the HAPPI experimental design as it allows us to isolate the direct effect of changing CO_2 on climate extremes. However, other possible experimental designs do exist where it would be possible to investigate this effect too[36,37]. In the setup described in reference [36], 1.5°C warming is arrived at by

2100 under two different emissions scenarios, one keeping concentrations below 440 ppm, and the other overshooting and then ramping down CO_2 concentrations to arrive at 1.5°C. In this setup however, there are many other differences between the simulations at 1.5°C, e.g. sea ice-cover, and so the setup makes it hard to disentangle the direct response on extremes due to differing atmospheric CO_2 concentrations. In the setup described in reference [37], first the CO_2 emissions are determined that drive a particular coupled model (CESM) to arrive at 1.5°C and 2.0°C global warming, and then the coupled model is run with this CO_2 concentration. Unlike the HAPPI setup, this guarantees the physically consistency of the setup and does not result in an SST response and CO_2 concentration that are potentially inconsistent. However, to then investigate the impact of changed atmospheric CO_2 concentration on extremes, one would then have to compare the impact across different models, making it hard to disentangle the direct effect of CO_2 from all the other differences that may give rise to that difference in sensitivity (e.g. model physics and SST anomaly pattern).

Regression model

To compute the contribution of changes in radiative forcing and changes in global mean temperature to a change in a particular variable, we fit the changes in the 10-year ensemble mean variables between present and 1.5°C runs to the model: $\Delta X = \alpha \Delta F + \beta \Delta \bar{T}$. ΔX is the change in variable. ΔF is the change in the radiative forcing due to CO_2 from the present decade, $\Delta F = \frac{3.71}{\ln 2} \cdot \ln\left(\frac{C}{C_p}\right)$[24] where C and C_p are the CO_2 concentration in the forced run and the present decade respectively in ppm. $\Delta \bar{T}$ is the change in global mean temperature between the 1.5°C ensembles and the present day ensemble (not the change in mean SST, thus $\Delta \bar{T}$ is different for the three 1.5°C ensembles). The regression framework allows us to account for the change in variables from the increase in global mean temperature arising from increased CO_2 concentrations, and so separate the effect of direct radiative CO_2 from the effect of the global mean temperature increase. The fit parameters α and β indicate the dependence of the change in variable to

changes in CO_2 radiative forcing and global mean temperature respectively. Uncertainty estimates in warming for a given radiative forcing are calculated from the covariance matrix of α and β which accounts for the spread in 10-year ensemble member mean quantities.

To apply the global mean temperature change correction, for each variable we subtract $\beta\,(\bar{T}_H - \bar{T}_{BE})$ from the high CO_2 ensemble variable, and add $\beta\,(\bar{T}_{BE} - \bar{T}_L)$ to the low CO_2 ensemble variable (subscripts: H - high ensemble, BE - best-estimate ensemble, L - low ensemble). For maps, β is calculated for each individual grid-point, for area mean indices, βs are calculated from the area mean of the variable in question.

Extreme indices

The extreme measures $\overline{TX90p}$ and $\overline{R95p}$ are taken from the dictionary of the European Climate Assessment and Dataset project (ECA&D), which has been commonly used in previous studies about climate extremes[38–40]. Precise definitions of the full list of indices are available at the ECA&D website (http://eca.knmi.nl/indicesextremes/indicesdictionary.php). The percentile thresholds for computing $\overline{TX90p}$ and $\overline{R95p}$ are calculated from the present day ensemble. Due to the quantity of daily data, we have not applied the five day filtering window when calculating the percentile threshold for $\overline{TX90p}$.

The simplified wet-bulb globe temperature (WBGT)[41] is given by: $WBGT = 0.567T + 0.393e + 3.94$, where T is the air temperature in degrees Celsius and e denotes the water vapour pressure in hPa. Water vapour pressure is calculated from relative humidity by $rH = \frac{e}{E} \times 100\%$. The saturation water pressure, E (in hPa), is approximated using the Magnus formula[42]: $E(T) = 6.112hPa \times \exp\left(\frac{17.62T}{243.12°C+T}\right)$. We define the index $\overline{WBGT95p}$ for a particular month as the number of degree months per year at each grid point above the 95th percentile of WGBT in the same month of the present day ensemble.

Significance testing

We test for a discernible signal against the decadal variability in the model by assessing the difference between the means of the two sets of 10 year extreme index means for each ensemble member. To test for discernible changes between the high and low CO_2 runs, the t-statistic does not depend on ensemble size, and is given by $t = \frac{\mu_h - \mu_l}{\sqrt{\sigma_h^2 + \sigma_l^2}}$, where the μ_i are the ensemble means in the high and low CO_2 cases, and the σ_i the standard deviations of the 10-year ensemble member means. This tests for a decadal signal against the internal variability inherent in the climate system. We assess discernibility at the 10% significance level. We also test for significant changes in the extreme index distributions using a two-sample Kolmogorov-Smirnov test at the 10% significance level.

Data availability

Model output data is being made available from the NERSC data portal: http://portal.nersc.gov/c20c/data.html.

References

27. Watanabe, M. *et al.* Improved Climate Simulation by MIROC5: Mean States, Variability, and Climate Sensitivity. *J. Clim.* **23**, 6312–6335 (2010). URL http://journals.ametsoc.org/doi/abs/10.1175/2010JCLI3679.1. DOI 10.1175/2010JCLI3679.1.

28. Gent, P. R. *et al.* The Community Climate System Model Version 4. *J. Clim.* **24**, 4973–4991 (2011). URL http://journals.ametsoc.org/doi/abs/10.1175/2011JCLI4083.1. DOI 10.1175/2011JCLI4083.1.

29. Pope, V. D., Gallani, M. L., Rowntree, P. R. & Stratton, R. A. The impact of new physical parametrizations in the Hadley Centre climate model: HadAM3. *Clim. Dyn.* **16**, 123–146 (2000). URL http://link.springer.com/10.1007/s003820050009. DOI 10.1007/s003820050009.

30. Gordon, C. *et al.* The simulation of SST, sea ice extents and ocean heat transports in a version of the Hadley Centre coupled model without flux adjustments. *Clim. Dyn.* **16**, 147–168 (2000). URL http://link.springer.com/10.1007/s003820050010. DOI 10.1007/s003820050010.

31. Guillod, B. P. *et al.* weather@home 2: validation of an improved global-regional climate modelling system. *Geosci. Model. Dev.* **10**, 1849–1872 (2017). URL https://www.geosci-model-dev.net/10/1849/2017/. DOI 10.5194/gmd-10-1849-2017.

32. Allen, M. Do-it-yourself climate prediction. *Nat.* **401**, 642–642 (1999). URL http://www.nature.com/doifinder/10.1038/44266. DOI 10.1038/44266.

33. Mitchell, D. *et al.* Half a degree Additional warming, Projections, Prognosis and Impacts (HAPPI): Background and Experimental Design. *Geosci. Model. Dev. Discuss.* **10**, 571–583 (2017). URL http://www.geosci-model-dev-discuss.net/gmd-2016-203/. DOI 10.5194/gmd-2016-203.

34. Massey, N. *et al.* weather@home-development and validation of a very large ensemble modelling system for probabilistic event attribution. *Q. J. R. Meteorol. Soc.* **141**, 1528–1545 (2015). URL http://doi.wiley.com/10.1002/qj.2455. DOI 10.1002/qj.2455.

35. Vogel, M. M. *et al.* Regional amplification of projected changes in extreme temperatures strongly controlled by soil moisture-temperature feedbacks. *Geophys. Res. Lett.* **44**, 1511–1519 (2017). URL http://doi.wiley.com/10.1002/2016GL071235. DOI 10.1002/2016GL071235.

36. Palter, J. B., Frölicher, T. L., Paynter, D. & John, J. G. Climate, ocean circulation, and sea level changes under stabilization and overshoot pathways to 1.5K warming. *Earth Syst. Dyn. Discuss.* 1–19 (2017). URL https://www.earth-syst-dynam-discuss.net/esd-2017-105/. DOI 10.5194/esd-2017-105.

438 **37.** Sanderson, B. M. *et al.* Community climate simulations to assess avoided impacts in 1.5 and 2C
439 futures. *Earth Syst. Dyn.* **8**, 827–847 (2017). URL https://www.earth-syst-dynam.net/
440 8/827/2017/. DOI 10.5194/esd-8-827-2017.

441 **38.** Frich, P. *et al.* Observed coherent changes in climatic extremes during the second half of the twentieth
442 century. *Clim. Res.* **19**, 193–212 (2002). URL http://www.int-res.com/abstracts/cr/
443 v19/n3/p193-212/. DOI 10.3354/cr019193.

444 **39.** Meehl, G. A. & Tebaldi, C. More Intense, More Frequent, and Longer Lasting Heat Waves in the 21st
445 Century. *Sci.* **305**, 994–997 (2004). URL http://science.sciencemag.org/content/
446 305/5686/994.full. DOI 10.1126/science.1098704.

447 **40.** Alexander, L. V. *et al.* Global observed changes in daily climate extremes of temperature and
448 precipitation. *J. Geophys. Res.* **111**, D05109 (2006). URL http://doi.wiley.com/10.1029/
449 2005JD006290. DOI 10.1029/2005JD006290.

450 **41.** Fischer, E. M. & Knutti, R. Robust projections of combined humidity and temperature extremes. *Nat.*
451 *Clim. Chang.* **3**, 126–130 (2012). URL https://www.nature.com/nclimate/journal/
452 v3/n2/pdf/nclimate1682.pdf. DOI 10.1038/NCLIMATE1682.

453 **42.** Sonntag, D. Important new values of the physical constants of 1986, vapor pressure formulations
454 based on ITS-90 and psychrometer formulae. *Zeitschrift für Meteorol.* **70**, 340–344 (1990).